Appl Phys A (2009) 96: 991–996
DOI 10.1007/s00339-009-5133-2

Applied Physics A
Materials Science & Processing

An investigation on magnetism, spin–phonon coupling, and ferroelectricity in multiferroic $GdMn_2O_5$

C.L. Lu · J. Fan · H.M. Liu · K. Xia · K.F. Wang · P.W. Wang · Q.Y. He · D.P. Yu · J.-M. Liu

Received: 18 January 2009 / Accepted: 26 January 2009 / Published online: 19 February 2009

Abstract The magnetization, Raman spectroscopy, and ferroelectricity of multiferroic $GdMn_2O_5$ as a function of temperature and magnetic field are investigated. The complicated magnetic transitions at low temperatures are featured with anomalous Raman mode shifts, dielectric response, and ferroelectricity generation, indicating the significant spin–phonon coupling. It is argued that this coupling is possibly responsible for the electrical polarization generation associated with the incommensurate–commensurate transition.

Keywords Multiferroic · Raman spectroscopy · Frustrated spin structure

PACS 77.80.-e · 75.30.Fv · 75.80.+q

1 Introduction

There is currently a new surge of interest in multiferroics which exhibit the coexistence of magnetism and ferroelectricity with crossing magnetoelectric (ME) coupling [1]. These materials are attractive due to the interesting physics involved and technologically important possibility for realizing the mutual controlling of electric and magnetic properties [2–5]. However, a number of multiferroics possess both ferroelectricity and magnetism but show a weak ME coupling [6]. The recently revived multiferroics $R\mathrm{MnO_3}$ [3, 4, 7, 8] and $R\mathrm{Mn_2O_5}$ [1, 2, 9–11] (R = Y, Tb, Dy, etc.) exhibit remarkable ME effect and seem to be promising candidates for understanding the fascinating physics and pushing the potential applications of multiferroics.

In fact, manganites with general formula $R\mathrm{Mn_2O_5}$ have been studied since the late 1960s [12]. These isostructure insulators consist of linked $\mathrm{Mn^{4+}O_6}$ octahedra and $\mathrm{Mn^{3+}O_5}$ pyramids in the orthorhombic *Pbam* structure. The octahedral share edges to form ribbons parallel to the c-axis, with the adjacent ribbons linked by pairs of corner-sharing pyramids [13], giving rise to five types of nearest-neighbor exchange interactions between Mn spins and thus the frustrated spin configuration. A delicate balance between these competing interactions is responsible for a cascade of magnetic phase transitions at various temperatures. It was speculated [14] that the electric polarization P, aligned along the b-axis, can be ascribed to the so-called magnetic Jahn–Teller (J–T) effect due to the antiferromagnetic (AFM) interactions dominating between the neighboring $\mathrm{Mn^{3+}}$ and $\mathrm{Mn^{4+}}$ ions within the a–b plane. In fact it was revealed experimentally that the onset of P always coincides with a commensurate (CM) magnetic ordering in multiferroics $R\mathrm{Mn_2O_5}$ (R = Tb, Dy, Ho, etc.) [2] instead of the incommensurate (ICM) ordering and spin noncollinearity which acts as key ingredient of multiferroic physics in $R\mathrm{MnO_3}$ (R = Gd, Tb, Dy, etc.) [3, 4, 7, 8, 15]. Therefore, for $R\mathrm{Mn_2O_5}$, it becomes critical to establish the correlation between the magnetic configuration and polarization generation.

C.L. Lu · J. Fan · H.M. Liu · K. Xia · K.F. Wang · J.-M. Liu (✉)
Nanjing National Laboratory of Microstructures, Nanjing University, Nanjing 210093, China
e-mail: liujm@nju.edu.cn

P.W. Wang · D.P. Yu
Electron Microscopy Laboratory, Peking University, Beijing 100871, China

Q.Y. He · J.-M. Liu
School of Physics, South China Normal University, Guangzhou 51006, China

J.-M. Liu
International Center for Materials Physics, Chinese Academy of Sciences, Shenyang, China

Nevertheless, the complex magnetic interactions in RMn_2O_5 make a detailed understanding of the multiferroic physics challenging. At this stage, a relatively simple system should be chosen for such a motivation. $GdMn_2O_5$, a member of the RMn_2O_5 family, has been paid little attention. It exhibits simpler multiferroic behavior than other systems (R = Tb, Dy, Ho) [16], although an investigation of the magnetic configuration becomes hard due to the very large neutron absorption cross section of rare earth ion Gd^{3+} [5, 16, 17]. Upon decreasing temperature T, $GdMn_2O_5$ undergoes an AFM transition at $T_N = 39$ K, and the spontaneous ferroelectric polarization (P) arises upon further cooling to $T_C = 25$ K [5, 16, 17]. The electric polarization is large and can be switched upon electric field reversal. However, no much investigation on the spin–phonon coupling or ME property in $GdMn_2O_5$ has been reported. In this work, we investigate the magnetism, Raman scattering spectroscopy, ferroelectric polarization, and dielectric susceptibility of $GdMn_2O_5$, in order to explore the spin–phonon coupling so that the origin of the ferroelectricity can be partially understood.

2 Experimental details

The single-phase polycrystalline $GdMn_2O_5$ was prepared by conventional solid-state reaction technique. The highly purified powders of oxides were mixed in stoichiometric ratios, ground and then fired at 1000°C for 24 hours (h) in an oxygen flow. The obtained powders were reground and compressed into pellets and then sintered at 1100°C for 24 h in an oxygen flow with intermediate grindings. The sample crystallinity was examined by X-ray diffraction (XRD) with Cu Kα radiation. The room temperature XRD pattern of $GdMn_2O_5$ shows that the sample is well crystallized and can be indexed by a pure orthorhombic structure adopting space group *Pbam*.

The magnetic measurements over a broad T-range were carried out using Quantum Design SQUID (superconducting quantum interfering device). In association with the magnetic data, we also perform Raman spectroscopy using a Renishaw in Via Raman microscope with an Ar ion laser (514 nm) source. The laser beam was focused by a microscope objective normal to the substrate surface down to a spot size of several microns in diameter. The emitted light was dispersed by an 1800 mm^{-1} grating and detected by a 1/4 in. format CCD with 3.2 mm × 2.4 mm slit size. The laser power was kept around 5 mW to avoid thermal effects. The temperature fluctuation due to the laser irradiation was ∼0.5 K. The dielectric susceptibility ε was measured using an HP4294A impedance analyzer connected with a Janis cryogenic system. The gold pastes were used as electrodes. To obtain the T-dependence of polarization P, the pyroelectric current was measured employing the Keithley 6514A electrometer while sweeping T at selected heating rates of 2 K/min and ∼4 K/min. The current measurement was performed by poling the sample at an electric field of ∼200 V/mm while cooling it down from a temperature $T = 100$ K $> T_N$. Before the measurement initiating at 3 K, the poling field was removed, and the sample was circuit-shortened for 1.5 hours so that the poling-induced charges are completely removed. The polarization P was then calculated by integrating the pyroelectric current.

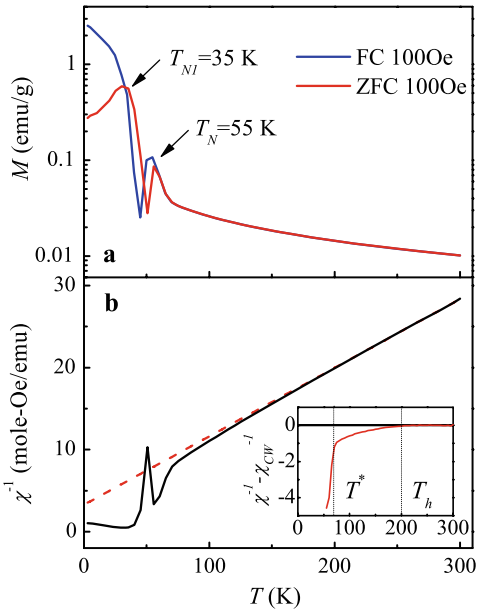

Fig. 1 (**a**) Measured M as a function of T in the ZFC and FC conditions. (**b**) Inverse dc magnetic susceptibility as a function of T (*black line*) measured under a field of 100 Oe, the *red dashed line* is the fitting following the Curie–Weiss law. The *inset* in (**b**) shows the inverse dc magnetic susceptibility as a function of T after subtract the *C–W* term above T_N, the *horizontal solid line* is a guide to the eyes. The *vertical dashed lines* in the *inset* of (**b**) mark the T^*, T_h, respectively

3 Results and discussion

3.1 Magnetic behavior

First, we look at the measured magnetization $M(T)$ with a magnetic field $H = 100$ Oe under zero-field cooling (ZFC) and field cooling (FC) conditions over a T-range of 3–300 K, as shown in Fig. 1(a). Two distinct magnetic transitions at $T = T_N \sim 55$ K and $T = T_{N1} \sim 35$ K are detected. The two transitions are respectively attributed to the long range AFM ordering of the Mn spins (i.e., at $T = T_N$) and the onset of the ferroelectric (FE) phase associated with the emergence of the CM phase (i.e., at $T = T_{N1}$), the latter indicating the coupling between the magnetic and ferroelectric

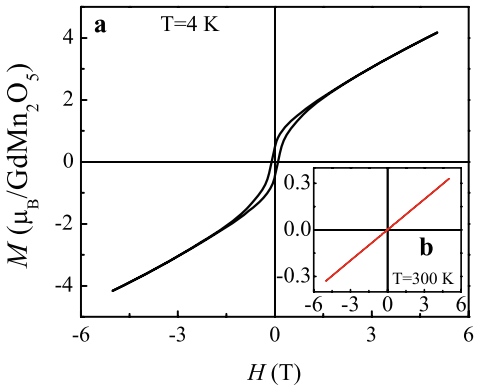

Fig. 2 Measured M as a function of H for $GdMn_2O_5$ at 4 K (**a**) and 300 K (**b**)

orders. These two transition points are slightly higher than those reported earlier [5, 16, 17]. In order to disclose the magnetic ordering over the whole T-range, we analyze the magnetic susceptibility χ in the ZFC case, and the data are presented in Fig. 1 (b). We employ the Curie–Weiss (C–W) law $\chi = C/(T - \theta_W)$, where C is the Curie constant, and θ_W the Curie temperature, to fit the data, generating $C = 11.7$ and $\theta_W = -39.7$ K. The negative θ_W indicates that the AFM order is favored. Just from this fitting, an effective magnetic moment of $\sim 9.7\mu_B$ per formal unit (f.u.) can be evaluated, which is larger than the expected value $\sim 8.77\mu_B$ per f.u., even assuming that the Mn spins are in perfectly parallel-aligned and each spin in a formal unit is a mixture of Mn^{3+} with moment of $4.90\mu_B$ and Mn^{4+} with moment of $3.87\mu_B$. Therefore, the fairly large magnetic moment per f.u. indicates the significant contribution of Gd^{3+} to the magnetic moment.

Second, the deviation of χ from the C–W law begins at $T = T_h \sim 200$ K, but a sudden increasing of this deviation occurs at $T = T^* \sim 70$ K $> T_N$, revealing that magnetic correlation (e.g., local spin order) is already established at a temperature as high as 200 K although T_N is only 55 K. This deviation can be seen more clearly in the inset of Fig. 1(b), which implies the existence of frustrated magnetic structure in $GdMn_2O_5$. This argument is additionally evidenced by the frustration factor $f = |\theta_W|/T_N \sim 1.0$, indicating the enhanced spin frustration tendency. In order to get further insight into the magnetic property in $GdMn_2O_5$, the H-dependence of M at 4 and 300 K was measured, as shown in Fig. 2 and the inset, respectively. The linear relationship between M and H at $T \sim 300$ K indicates a paramagnetic behavior at this T. However, in contrast, an evident hysteresis in the M–H curve can be seen at 4 K, and the $M(H)$ does not show any saturation till a field as high as 5 Tesla (T). This feature supports the augment of an inherent frustrated magnetic structure in $GdMn_2O_5$.

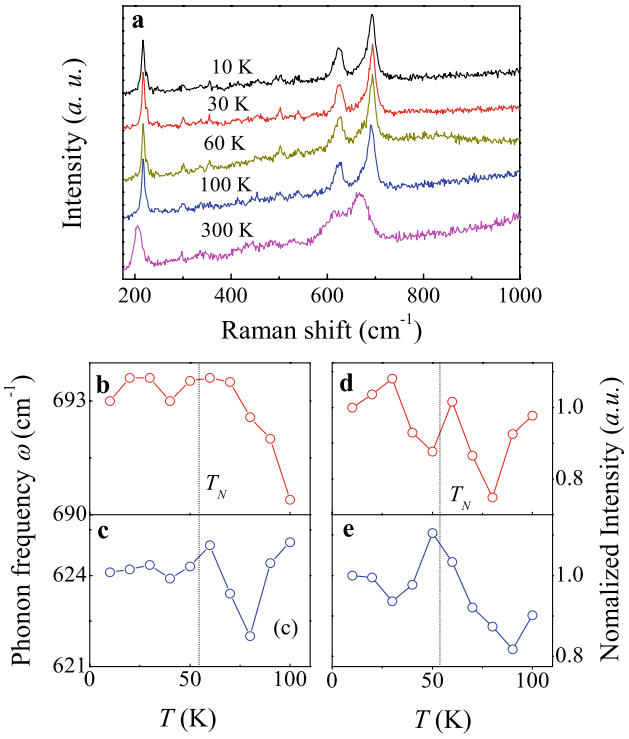

Fig. 3 (**a**) Unpolarized Raman spectroscopy for $GdMn_2O_5$, (**b**) and (**c**) T-dependence of the frequency of selected Raman modes, (**d**) and (**e**) T-dependence of the Raman scattering intensity of the peak around 616 cm^{-1} and 667 cm^{-1}, respectively. The *vertical dashed lines* in (**b**)–(**e**) mark the T_N

3.2 Raman spectroscopy

To reveal the nature of the magnetic correlation far above T_N evidenced above and, more importantly, the magnetic coupling with possible ferroelectric order, the Raman scattering spectroscopy at different T was performed, so that the spin–phonon coupling and phonon mode softening/hardening can be revealed. Figure 3(a) shows the unpolarized Raman scattering spectra at $T = 10$, 30, 60, 100, and 300 K. The overall Raman scattering is very similar to that of (Dy, Eu)Mn_2O_5. With decreasing T, the Raman-active phonon modes become sharper and well defined, especially the high-energy modes at ~ 616 and ~ 667 cm^{-1}, which are ascribed to the Mn–O stretching vibrations [18]. Referring to the spectrum from the paraelectric phase, no new Raman peak was observed at $T < T_{N1}$. This suggests that the ionic displacements associated with the ferroelectric phase is rather small, confirmed by the very small polarization to be shown below.

To illustrate the spin–phonon coupling in a clear manner, we plot the T-dependence of phonon frequency (ω) and intensity of the high-energy modes in Figs. 3(b)–(e), respectively. An anomalous phonon behavior, as a function of T, is identified. For the mode at ~ 667 cm^{-1}, phonon frequency ω shows the conventional mode hardening upon decreasing of T down to ~ 70 K $> T_N$ and then becomes saturated upon

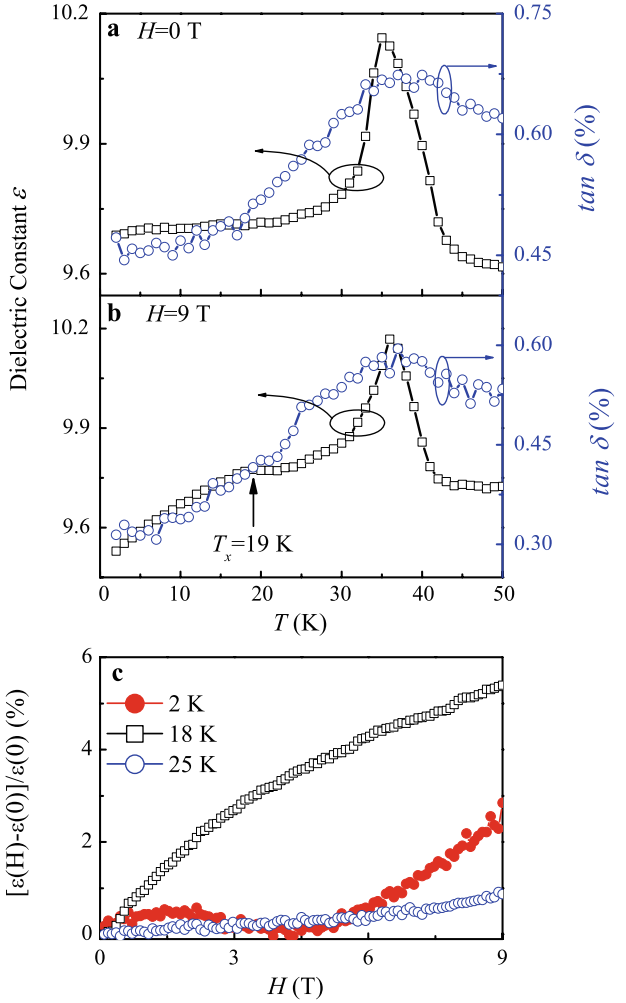

Fig. 4 (**a**) T-dependence of dielectric constant ε and $\tan\delta$ at 1 MHz under $H = 0$; (**b**) T-dependence of dielectric constant ε and $\tan\delta$ at 1.0 MHz under $H = 9$ T; (**c**) Change of dielectric constant $\Delta\varepsilon/\varepsilon_0$ vs. H at $T = 2$, 18, and 25 K, measured under the ZFC condition

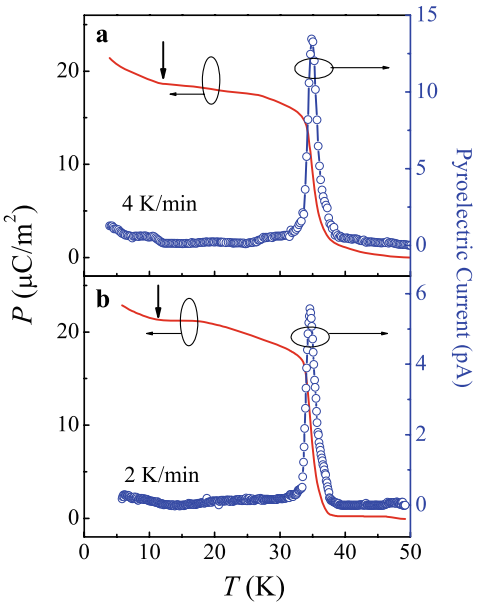

Fig. 5 T-dependence of polarization P and pyroelectric current I under $H = 0$. The heating rate is (**a**) 4 K/min, and (**b**) 2 K/min

further cooling. However, for the mode at ~616 cm^{-1}, frequency ω exhibits distinct and anomalous softening at $T \sim 100$ K $> T_N$. Around $T = T_N$, there occurs possibly another anomalous softening. The anomalous feature above T_N can be also observed in the T-dependence of the phonon mode intensity, as shown in Figs. 3(d) and (e). The intensity is normalized by the Bose factor $n + 1 = (1 - \exp(-\hbar\omega/kT))^{-1}$, where $\hbar$ is the Plank constant, and k is Boltzmann constant, and by the intensity of the corresponding modes at ~10 K [19]. In addition, anomalies around T_N and T_{N1} in the T-dependence of intensities of the two modes at ~667 and ~616 cm^{-1} can be identified, confirming the significant spin–phonon coupling.

3.3 Dielectric and ferroelectric behavior

Keeping in mind the complicated magnetic ordering sequence and spin–phonon coupling, we then look at the T-dependence of dielectric constant ε and ferroelectric polarization P, which may also exhibit anomalies at the magnetic transition points if any coupling between the magnetic and ferroelectric orders is available. We measure the magnetodielectric behaviors expressed by $\varepsilon(T, H)$ around T_C and below, and the corresponding ferroelectric polarization P. The measured data are presented in Figs. 4 and 5 for $T = 2$~50 K and $H = 0$~9 T. For the response of P to magnetic field, it was observed that P rapidly falls down to zero or very low values which cannot be measured reliably. We then focus on the dielectric response shown in Fig. 4.

As expected, at $H = 0$, $\varepsilon(T)$ shows a sharp peak at $T \sim 35$ K, and in correspondence, $\tan\delta(T)$ also shows a peak around this point. This feature reflects the occurrence of ferroelectric transition at $T_C \sim 35$ K, perfectly consistent with the anomaly of $M(T)$ at $T_{N1} \sim 35$ K below T_N, indicating the coupling between magnetism and ferroelectricity. With increasing field H, there appears a shoulder in the left side of T_C for $\varepsilon(T)$. This shoulder becomes more significant with increasing H until a field as large as 9 T, at which a step-like anomaly of $\varepsilon(T)$ at $T = T_x \sim 19$ K can be identified, as shown in Fig. 4 (b).

To precisely characterize the evolution of the dielectric behavior with H, we measured the variation of dielectric constant $\Delta\varepsilon/\varepsilon_0$ as a function of H at $T = 2$, 18, and 25 K. The data are plotted in Fig. 4(c). The measured $\Delta\varepsilon(H)/\varepsilon_0$ at both $T = 25$ and 18 K is a monotonous function of H, although a much larger ME effect can be seen at $T = 18$ K. However, the data of $\Delta\varepsilon(H)/\varepsilon_0$ at $T = 2$ K seem to be more complex, and a broad peak of $\varepsilon(H)$ appears around $H \sim 2$ T. This broad peak diminishes at a temperature higher than the

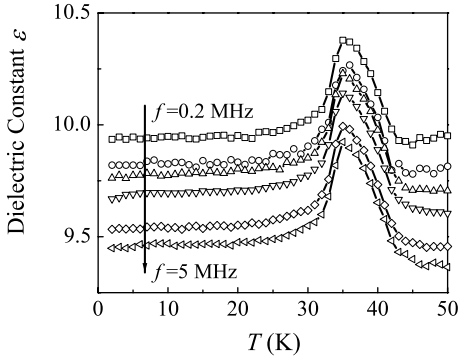

Fig. 6 T-dependence of dielectric constant ε at various frequencies, 0.3, 0.5, 0.8, 1.0, 3.0, 5.0 MHz, under $H = 0$

magnetic ordering point of Gd ions, suggesting its correlation with the ordering of Gd spins [17].

The T-dependence of polarization and pyroelectric current I measured at different warming rates are presented in Fig. 5. $P(T)$ exhibits a quick increase around $T \sim 35$ K, and a sharp peak at $T \sim 35$ K can be seen in I(T), both of which are consistent with the anomaly of $\varepsilon(T)$ at $T_C = 35$ K. There is another distinct increase in $P(T)$ at ~12 K, indicated by black arrows in Fig. 5, which can be associated with the magnetic ordering of Gd ions [5, 17]. In addition, the peak in $I(T)$ shows no shift as the heating rate varied from 2 to 4 K/min, indicating that the anomaly at T_C indeed results from the spin–phonon coupling instead of the discharge of a trap level possibly existing in the band gap. To further confirm this point, T-dependence of dielectric constant ε at several selected frequencies was measured, as shown in Fig. 6. It is noted that a trap level will be active at frequency below few tens of kHz, whereas the characteristic frequency for the spin–phonon coupling would be well larger than ~MHz range. Actually, the anomaly of $\varepsilon(T)$ at T_C remains clearly identifiable as the frequency is as large as 5 MHz, indicating the true spin–phonon coupling mechanism.

3.4 Discussion

The above investigation on $GdMn_2O_5$ shows some interesting phenomena outlined here: (i) the frustration factor $f = |\theta_W|/T_N \approx 1$ confirms the magnetic frustration; (ii) the magnetic susceptibility shows distinct deviation from the C–W law, and anomalous phonon shift is observed far above T_N, indicating the magnetic correlations in the paramagnetic (PM) phase for its inherent magnetic frustration; (iii) the obvious spin–phonon coupling effect, and a characteristic temperature $T = T_x \sim 19$ K observed in the $\varepsilon(T, H)$ curve under a magnetic field of 9 T. These effects can be qualitatively understood based on the spin–phonon coupling mechanism.

For magnetic materials, the phonon frequency is sensitive to the nearest-neighboring spin correlations. To the first-order approximation, this dependence can be described by $\omega = \omega_0 + \lambda\langle S_i \cdot S_j\rangle$, where ω_0 is the phonon frequency, and $\langle S_i \cdot S_j\rangle$ is the spatial spin correlation function [20]. For multiferroics RMn_2O_5, the high-frequency phonons were ascribed to the Mn–O stretching vibrations which are apt to modulate the Mn–O–Mn superexchange interactions. Therefore, the anomalous phonon shift above T_N together with the deviation of the magnetic susceptibility from the C–W law is the outcome of the strong spin–phonon coupling in $GdMn_2O_5$ [20], noting that strong spin–phonon coupling has also been observed in other multiferroics RMn_2O_5 (R = Bi, Eu, and Dy) [18].

To understand the physics underlying the ME effects, we note that the dependence of dielectric susceptibility on the spin configuration is similar to that for the phonon model shift. We may express this dependence as $\varepsilon(T, H) = \varepsilon_0(T)(1 + \alpha\langle S_i \cdot S_j\rangle)$, which is naturally based on the spin–phonon coupling, as investigated in $EuTiO_3$ [21]. The emergence of T_x is intrinsically associated with a field-induced magnetic transition in $GdMn_2O_5$. We note that the single-crystal data revealed that H-dependence of isothermal P shows only slight change at small field. However, a clear jump of P arises at H and is as high as 8 T [5]. This change cannot be only ascribed to a subtle variation of the spin configuration but should be associated with a magnetic transition. Considering the fact that the CM magnetic modulation is an essential ingredient of ferroelectricity generation [9, 11], we argue that the dielectric anomaly arising at $T = T_x \sim 19$ K is an indicator of field-induced ICM–CM transition.

4 Conclusion

In summary, we have studied the magnetic properties, Raman scattering spectra, ferroelectric polarization, and dielectric susceptibility as a function of T and H in $GdMn_2O_5$. The Curie–Weiss fitting of the T-dependent dc susceptibility reveals that the magnetic correlation ensues far above T_N due to the inherent magnetic frustration. Simultaneously, the anomalous phonon shifts above T_N by the Raman spectroscopy have been observed. The correspondence between the ferroelectric and dielectric responses and the complicated magnetic transitions has been established. These phenomena can be interpreted based on the spin–phonon coupling.

Acknowledgements The authors thank the National Natural Science Foundation of China (50832002, 10674061, 50601013, 10874075) and National Key Projects for Basic Research of China (2009CB623303, 2009CB929501).

References

1. N. Hur, S. Park, P.A. Sharma, J.S. Ahn, S. Guha, S.-W. Cheong, Nature **429**, 392 (2004)

2. S.-W. Cheong, M. Mostovoy, Nat. Mater. **6**, 13 (2007)
3. T. Kimura, T. Goto, H. Shintani, K. Ishizaka, T. Arima, Y. Tokura, Nature **426**, 55 (2003)
4. T. Lottermoser, T. Lonkai, U. Amann, D. Hohlwein, J. Ihringer, M. Fiebig, Nature **430**, 541 (2004)
5. A.M. Kadomtseva, S.S. Krotov, Y.F. Popov, G.P. Vorob'ev, Low Temp. Phys. **32**, 709 (2006)
6. H. Béa, M. Bibes, S. Fusil, K. Bouzehouane, E. Jacquet, K. Rode, P. Bencok, A. Barthélémy, Phys. Rev. B **74**, 020101(R) (2006)
7. D. Lee, J.-H. Lee, P. Murugavel, S.Y. Jang, T.W. Noh, Y. Jo, M.-H. Jung, Y.D. Ko, J.-S. Chung, Appl. Phys. Lett. **90**, 182504 (2007)
8. L.J. Wang, S.M. Feng, J.L. Zhu, R.C. Yu, C.Q. Jin, W. Yu, X.H. Wang, L.T. Li, Appl. Phys. Lett. **91**, 172502 (2007)
9. C.R. dela Cruz, B. Lorenz, Y.Y. Sun, Y. Wang, S. Park, S.-W. Cheong, M.M. Gospodinov, C.W. Chu, Phys. Rev. B **76**, 174106 (2007)
10. N. Hur, S. Park, P.A. Sharma, S. Guha, S.-W. Cheong, Phys. Rev. Lett. **93**, 107027 (2004)
11. D. Higashiyama, S. Miyasaka, Y. Tokura, Phys. Rev. B **72**, 064421 (2005)
12. G. Buisson, Phys. Status Solidi A **17**, 191 (1973)
13. G.R. Blake, L.C. Chapon, P.G. Radaelli, S. Park, N. Hur, S.-W. Cheong, J. Rodríguez-Carvajal, Phys. Rev. B **71**, 214402 (2005)
14. L.C. Chapon, G.R. Blake, M.J. Gutmann, S. Park, N. Hur, P.G. Radaelli, S.-W. Cheong, Phys. Rev. Lett. **93**, 177402 (2004)
15. S. Dong, R. Yu, S. Yunoki, J.-M. Liu, E. Dagotto, Phys. Rev. B **78**, 155121 (2008)
16. A. Inomata, K. Kohn, J. Phys., Condens. Matter **8**, 2673 (1996)
17. E. Golovenchits, V. Sanina, J. Phys., Condens. Matter **16**, 4325 (2004)
18. A.F. García-Flores, E. Granado, H. Martinho, R.R. Urbano, C. Rettori, E.I. Golovenchits, V.A. Sanina, S.B. Oseroff, S. Park, S.-W. Cheong, Phys. Rev. B **73**, 104411 (2006)
19. D.A. Tenne, A. Bruchhausen, N.D. Lanzillotti-Kimura, A. Fainstein, R.S. Katiyar, A. Cantarero, A. Soukiassian, V. Vaithyanathan, J.H. Haeni, W. Tian, D.G. Schlom, K.J. Choi, D.M. Kim, C.B. Eom, H.P. Sun, X.Q. Pan, Y.L. Li, L.Q. Chen, Q.X. Jia, S.M. Nakhmanson, K.M. Rabe, X.X. Xi, Science **313**, 1614 (2006)
20. A.B. Sushkov, O. Tchernyshyov, W. Ratcliff II, S.W. Cheong, H.D. Drew, Phys. Rev. Lett. **94**, 137202 (2005)
21. T. Katsufuji, H. Takagi, Phys. Rev. B **64**, 054415 (2001)